Title:

Synaptic Location Is a Determinant of the Detrimental Effects of α-Synuclein Pathology to Glutamatergic Transmission in the Basolateral Amygdala

Chetan Nagaraja*, Liqiang Chen*, Samuel Daniels*, Lindsay Meyerdirk, Jennifer A Steiner, Martha L. Escobar Galvis, Michael Henderson, Patrik Brundin, Hong-Yuan Chu

Department of Neurodegenerative Science, Parkinson's Disease Center, Van Andel Institute

* These authors contributed equally to this work

Address

333 Bostwick Ave NE, Grand Rapids, MI, 49503, USA

Correspondence

Hongyuan.chu@vai.org

Author contributions.

C.N., L.C., and S.D., investigation, formal analysis; L.M., M.H., J.A.S, and P.B, resources; H.Y.C., conceptualization; H.Y. C: writing– original draft; M.L.E.G, M.H., P.B. and H.Y.C., writing– review and editing; H.Y.C., supervision and funding acquisition. All authors reviewed and approved the manuscript.

Acknowledgement

This work was supported by the NARSAD Young Investigator award from the Brain and Behavior Research Foundation (H.Y.C) and an investigator-initiated research award from the Department of Defense (W81XWH2110943, PI: H.Y.C). Dr. Hong-Yuan Chu is a Frederick & Alice Coles and Thomas & Nancy Coles Investigator. The authors thank the Van Andel Institute Optical Imaging Core for the advanced confocal microscopy. The authors thank the Van Andel Institute Vivarium and Transgenics Core, especially Megan Tompkins, Alyssa Bradfield, and Malista Powers, for animal husbandry and colony maintenance.

Conflicts of interest

P.B. has consulted for Axial Therapeutics, Calico, CuraSen, Enterin Inc, Fujifilm-Cellular Dynamics Inc, Idorsia and Lundbeck A/S. He has received commercial support for research from Lundbeck A/S and Roche, and has ownership interests in Acousort AB, Axial Therapeutics, Enterin Inc. and RYNE Biotechnology Inc.

Abstract

α-Synuclein (αSyn) is a soluble protein enriched at presynaptic boutons and its abnormal aggregation is a hallmark of Parkinson's disease (PD). The amygdala shows selective vulnerability to the formation of insoluble αSyn aggregates, and its circuit dysfunction may contribute to prevalent psychiatric deficits in PD. Yet, how αSyn aggregates affect the amygdala function remains elusive. In the present study, we examined the presence of αSyn in glutamatergic axon terminals and how its aggregation affects glutamatergic transmission in the basolateral amygdala (BLA). Using confocal microscopy, we showed that αSyn is primarily present in the axon terminals expressing vesicular glutamate transporter 1 (vGluT1), but not in those expressing vGluT2. Using electrophysiology and optogenetics, we found that glutamatergic neurotransmission from vGluT1^{+} axon terminals are functionally more vulnerable than vGluT2^{+} axon terminals to the toxic effects of pathological αSyn aggregation triggered by αSyn preformed fibrils (PFFs). Using the PFFs models and mouse genetics, we showed that loss of αSyn promotes short-term depression of cortico-BLA synapses responding to repetitive stimuli, leading to an input-selective filtering of cortical inputs to the BLA. Together, we demonstrate that αSyn expresses specifically in a subset of synapses in mouse amygdala, which causes an input-specific decrease of cortical inputs to the BLA as αSyn aggregation forms. These results might be relevant to the reduced cortical control of amygdala function that has been associated with psychiatric deficits in PD.

Introduction

α-Synuclein (αSyn) is a soluble protein abundant at presynaptic axon terminals, where it regulates the dynamics of synaptic vesicles through interaction with synaptic proteins and presynaptic membranes (Burré et al., 2010; Runwal and Edwards, 2021; Vargas et al., 2017). αSyn is also prone to aggregation and aggregated αSyn is the major protein component of Lewy pathology seen in synucleinopathies like Parkinson's disease (PD) (Mezey et al., 1998; Spillantini et al., 1997). Moreover, increasing evidence supports the notion that pathologic αSyn propagates between synaptically interconnected brain regions and underlies PD progression (Angot et al., 2010; Luk et al., 2012; Uemura et al., 2020).

The amygdala is a key limbic structure for emotion regulation (Janak and Tye, 2015). Compelling clinical evidence indicates that cortical control of the amygdala activity is impaired in PD, leading to an inappropriate encoding of emotion valence or deficits in linking emotion to proper behavior (Bowers et al., 2006; Hu et al., 2015; Yoshimura et al., 2005). Moreover, the amygdala consistently shows selective vulnerability to Lewy pathology (Harding et al., 2002; Nelson et al., 2017; Sorrentino et al., 2019), thus an impaired amygdala network function has been proposed to underlie the disrupted emotion processing in PD patients (Harding et al., 2002). Still, the normal function of αSyn and how its aggregation can impair circuit function in the amygdala remain poorly understood. Here, we show that αSyn is primarily present in vesicular glutamate transporter 1-expressing (vGluT1$^+$) cortical axon terminals, being barely detectable in vGluT2-expressing (vGluT2$^+$) thalamic axon terminals in the basolateral amygdala (BLA). Using an αSyn preformed fibrils (PFFs) model of synucleinopathy, we

also show that development of αSyn pathology disrupts vGluT1^{+} cortico-BLA glutamatergic transmission, without affecting the vGluT2^{+} thalamo-BLA neurotransmission. Combining optical imaging with physiological approaches, we demonstrate that a partial (secondary to αSyn aggregation) or complete depletion of soluble αSyn (*Snca* KO mice) from the axon boutons promotes short-term depression at cortico-BLA synapses in response to prolonged stimulation, leading to an impaired gain control of cortical inputs to the BLA. Therefore, we conclude that changes in αSyn function decrease the cortical inputs to the BLA in an input-specific manner. Our data support clinical observations of an impaired cortical control of the amygdala activity that could contribute to psychiatric deficits of PD patients.

Results and Discussion

αSyn localizes preferentially in vGluT1⁺ axon terminals in mouse brain

Compelling evidence from PD patients suggests that the amygdala exhibits an impaired responsiveness to sensory stimuli, arising mainly from the cerebral cortex and the thalamus (Bowers et al., 2006; Hu et al., 2015). Since the cortical and thalamic glutamatergic axon terminals express vGluT1 and vGluT2, respectively (Fremeau et al., 2001; Kaneko and Fujiyama, 2002; Vigneault et al., 2015), we examined the presence of αSyn in vGluT1⁺ and vGluT2⁺ axon buttons in WT mouse brains. Figure 1 shows that αSyn immunoreactivity colocalizes with vGluT1⁺ puncta but is absent where there are vGluT2⁺ puncta, in the BLA, the cerebral cortex, and the striatum. It suggests that αSyn preferentially presents at vGluT1⁺ axon terminals arising from cortical regions. This observation is consistent with previous *in situ* hybridization studies showing higher αSyn mRNA expression in the cerebral cortex and the hippocampus than in the thalamus (Abeliovich et al., 2000; Ziolkowska et al., 2005).

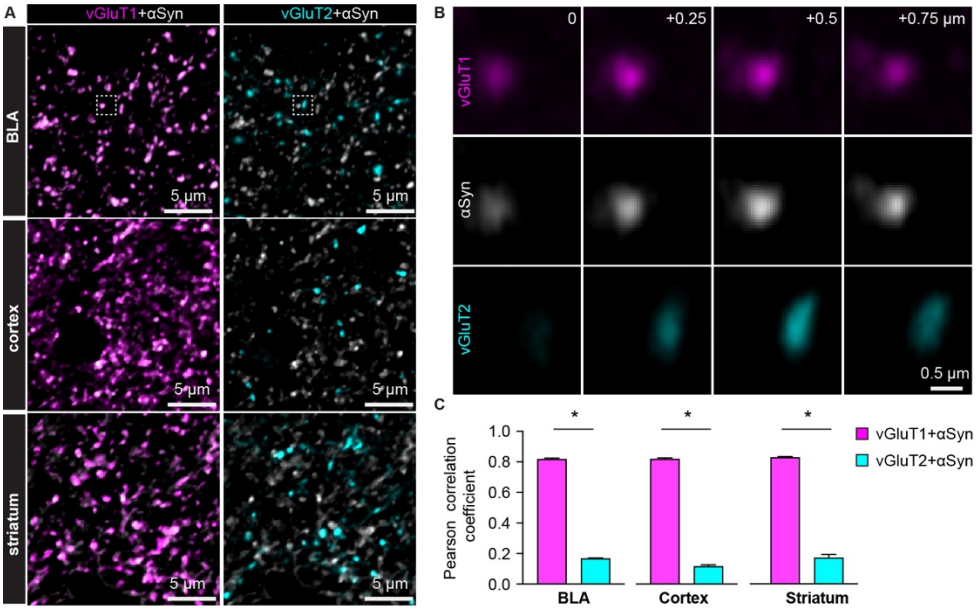

Figure 1. αSyn is selectively localized at vGluT1⁺ axon terminals in mouse brain. A) Representative confocal images showing colocalization of αSyn with vGluT1 (left), but not with vGluT2 (right) in the BLA (top), cerebral cortex (middle), and the striatum (bottom). Simultaneously collected confocal images from each brain region were split into vGluT1/αSyn and vGluT2/αSyn channels for the purpose of illustration. **B**) Zoomed z series of images of the boxed area from the BLA in (A) showing colocalization and correlated changes in the immunoreactive intensities of vGluT1 and αSyn. Such colocalization and correlation is absent between vGluT2 and αSyn within the same region. Images were taken and shown from a 0.75 µm z-depth with an inter-section interval of 0.25 µm. **C**) Bar graphs showing Pearson correlation coefficient between vGluT1 and αSyn, as well as between vGluT2 and αSyn, in the BLA (αSyn/vGluT1 = 0.82±0.007, αSyn/vGluT2 = 0.17±0.004; n = 18 slices/4 mice; $p<0.05$, MWU), cerebral cortex (αSyn/vGluT1 = 0.82±0.006, αSyn/vGluT2 = 0.12±0.009; n = 8 slices/3 mice; $p< 0.05$, MWU), and the striatum (αSyn/vGluT1 = 0.83±0.006, αSyn/vGluT2 = 0.17±0.02; n = 8 slices/3 mice; $p< 0.05$, MWU).

Glutamate release from vGluT1⁺ axon terminals is selectively disrupted by αSyn pathology

Considering that αSyn is selectively present in vGluT1⁺ axon terminals, and that the endogenous αSyn is a determinant of the propensity to form αSyn aggregation, one can hypothesize that these terminals are more susceptible to the detrimental effects of αSyn pathology compared to vGluT2⁺ terminals (Erskine et al., 2018; Vasili et al., 2022). To test this hypothesis, we triggered αSyn pathology in the brain using the intrastriatal PFFs seeding model (Luk et al., 2012). One-month post-injection, we detected robust αSyn pathology in vGluT1⁺ cerebral cortical regions (e.g., the temporal association cortex (TeA) and the perirhinal cortex), but we barely observed any cytoplasmic aggregates in vGluT2⁺ thalamic regions (data not shown), which is consistent with earlier reports (Burtscher et al., 2019; Henderson et al., 2019; Luk et al., 2012; Stoyka et al., 2019). These findings are also expected considering the low level, or even

absence of αSyn mRNA expression in vGluT2$^+$ thalamic regions (Abeliovich et al., 2000; Ziolkowska et al., 2005).

The cerebral cortex and thalamus provide major excitation to the BLA for emotion regulation, thus we further examined whether vGluT1$^+$ cortico-BLA and vGluT2$^+$ thalamo-BLA synaptic transmission are differentially affected by αSyn pathology. We activated cortical and thalamic inputs of the BLA selectively by stimulating the external and internal capsules, respectively. One-month post-injection, the amplitude of electrically evoked cortico-BLA EPSCs was greatly decreased in the slices from PFFs-injected WT mice relative to those from controls (Figure 2A, B). In contrast, there was no difference in the amplitude of thalamo-BLA EPSCs between the PFFs-injected mice and controls (Figure 2C, D).

To avoid potential technical issues in the use of electrical stimulation, we employed optogenetic approach to confirm the above results (Figure 2E-J). One-month post-injection, the amplitude of optogenetically-evoked cortico-BLA EPSCs in slices from PFFs-injected mice was decreased relative to those from PBS-injected controls (Figure 2K, L). By contrast, we detected no difference in the amplitude of optogenetically-evoked thalamo-BLA EPSCs between groups (Figure 2M, N). Altogether, we demonstrated that the presence of αSyn makes vGluT1$^+$ axon buttons more vulnerable to αSyn pathology after injection of PFFs and that this pathology is associated with detrimental effects on synaptic transmission.

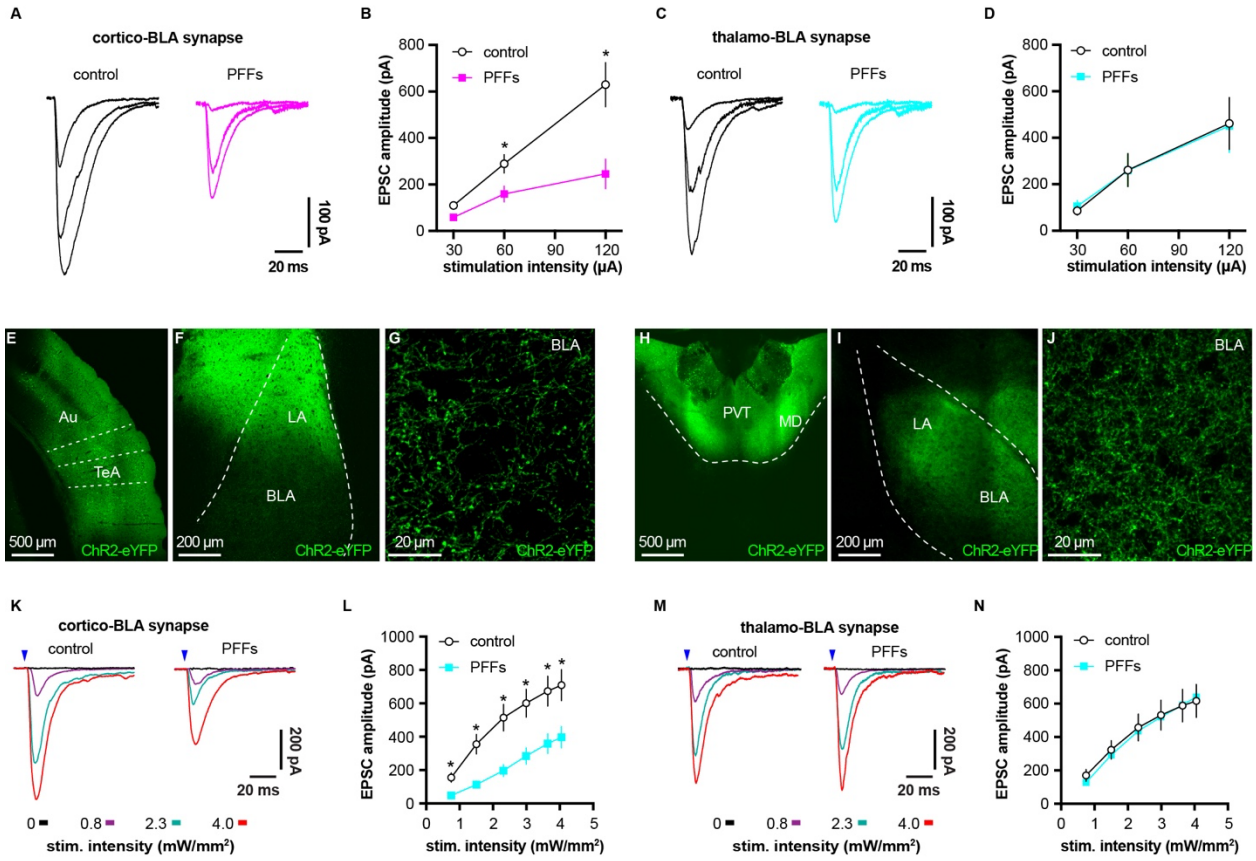

Figure 2. αSyn aggregates preferentially disrupt vGluT1⁺ cortico-BLA transmission. A-B) Representative traces of EPSCs evoked by electrical stimulation of the external capsule (A) and summarized results (B) showing a reduced cortico-BLA transmission in slices from PFFs- versus PBS-injected mice. n = 17 neurons/4 mice for each group. **C-D**) Representative traces of EPSCs evoked by electrical stimulation of the internal capsule (C) and summarized results (D) showing unaltered thalamo-BLA transmission in slices from PFFs- versus PBS-injected wildtype mice. n = 17 cells/5 mice for controls, and 13 cells/4 mice. **E-G**) Representative images showing viral infection site in the TeA and nearby regions (E), and the axon terminal field in the BLA under low (F) and high (G) magnification. **H-J**) Representative images showing viral infection site in the midline thalamus (H), and the axon terminal field in the BLA under low (I) and high (J) magnification. **K-L**) Representative traces of optogenetically-evoked EPSCs (K) and summarized results (L) showing a reduced amplitude of cortico-BLA EPSCs in slices from PFFs- versus PBS-injected mice. n = 35-37 neurons/4 mice. **M-N**) Representative traces of optogenetically-evoked EPSCs (M) and summarized results (N) showing unaltered thalamo-BLA transmission in slices from PFFs- versus PBS-injected mice. n = 28 neurons/4 mice. *, p< 0.05, MWU followed by Bonferroni-Dunn correction for multiple comparisons.

Consistent with the development of αSyn pathology following PFFs injection requiring the presence of endogenous αSyn (Luk et al., 2012; Volpicelli-Daley et al., 2011), we did not detect difference in the cortico-BLA transmission between PFFs- versus PBS-injected αSyn KO mice (data not shown). Because of the lack of detrimental effect in αSyn KO mice, we conclude that the impaired cortico-BLA transmission in the PFFs model is likely to be caused by the gained toxic properties of αSyn as it aggregates (Cookson and Brug, 2008; Volpicelli-Daley et al., 2011).

These results further highlight the dependence of regional and cellular vulnerability on the endogenous αSyn, i.e., those neurons or axon terminals that express high levels of αSyn are prone to be functionally impacted by αSyn pathology relative to those which lack of or express low levels of αSyn (Surmeier et al., 2017; Thakur et al., 2019; Vasili et al., 2022). Of particular interest is that $vGluT2^{+}/TH^{+}$ midbrain dopamine neurons and their axon terminals in the striatum are more resilient to neurodegeneration in postmortem PD brains and animal models studies (Buck et al., 2021; Thomas et al., 2021). While several other mechanisms have been proposed (Buck et al., 2021), the absence of αSyn at $vGluT2^{+}$ neurons/terminals could be critical for such resilience.

Pathological aggregation decreases αSyn levels at axon terminals and impairs short-term synaptic plasticity

Formation of cytoplasmic aggregates is believed to move soluble αSyn away from the presynaptic buttons, affecting its role in regulating synaptic vesicle pools (Benskey et al., 2016; Volpicelli-Daley et al., 2011). Consistent with the earlier

predictions, the intensity of αSyn immunoreactivity within vGluT1^{+} puncta decreased dramatically as αSyn pathology develops in our PFFs model, leading to an increased proportion of vGluT1^{+} buttons that lack detectable level of αSyn (Figure 3). These data suggest that αSyn pathology reduces the amount of αSyn present at the cortical axon terminals in the BLA, and in that way could affect its physiological function.

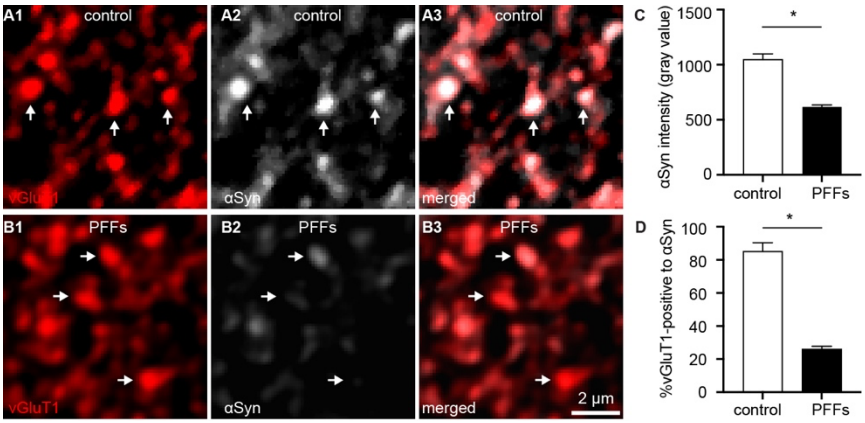

Figure 3. Decreased αSyn levels at axon terminals as it forms aggregates. A1-B3) Representative confocal images showing immunoreactivity of αSyn that is localized within vGluT1 immunoreactive puncta in BLA slices from a control (A1-A3) and PFFs-injected mouse (B1-B3). **C**) Summarized graph showing a reduced αSyn immunoreactivity per vGluT1 immunoreactive puncta in PFFs-injected mice relative to controls (control = 1049±50; PFFs = 617±18, n = 100 puncta/group, $p < 0.0001$, MWU). **D**) Summarized graph showing a reduced percentage of vGluT1 immunoreactive puncta associated with detectable αSyn immunoreactivity in PFFs-injected mice relative to controls (controls = 85±5.2%; PFF = 26±1.7%, n= 6 slices/group, $p = 0.002$, MWU).

αSyn modulates the dynamics of synapse vesicle pools (Sulzer and Edwards, 2019), which plays a key role in regulating synaptic plasticity and the computational function of neural circuits (Abbott and Regehr, 2004; Alabi and Tsien, 2012). Thus, we stimulated cortico-BLA synapses repetitively to assess the impact of the observed reduction of αSyn levels on short-term synaptic plasticity. We detected a progressive

depression of cortico-BLA EPSCs in control mice (Figure 4A1, A2), reflecting mainly a progressive depletion of presynaptic vesicles (Alabi and Tsien, 2012; Cabin et al., 2002). Interestingly, the cortico-BLA EPSCs in the slices from PFFs-injected mice showed a greater depression relative to those from controls (Figure 4A1, A2). These results are in line with the key role of αSyn in sustaining and mobilizing synaptic vesicle pools (Cabin et al., 2002; Sulzer and Edwards, 2019; Vargas et al., 2017), and suggest the significant impact of the loss of αSyn function on synaptic plasticity and circuit computation.

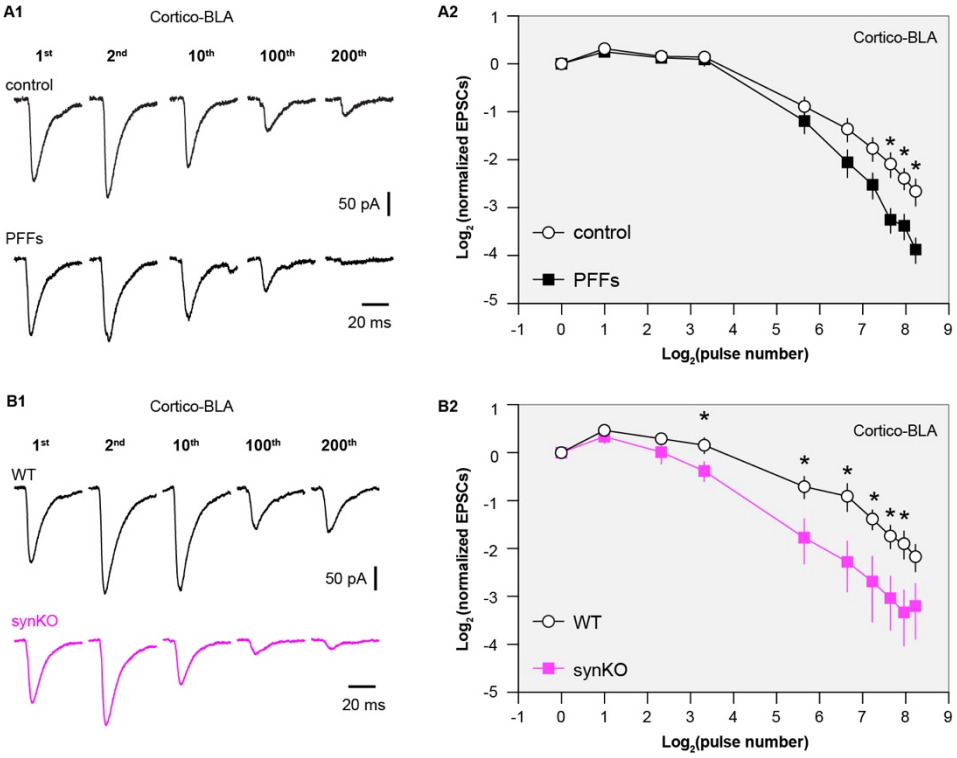

Figure 4. Loss of αSyn impairs short-term plasticity of the cortico-BLA inputs. A1) Representative cortico-BLA EPSCs traces from control and PFF-injected mice in response to repetitive stimulation (300 stimuli at 12.5 Hz). **A2**) Summarized graph showing the temporal profiles of cortico-EPSCs depression in slices from control and PFFs-injected mice. The cortico-BLA EPSCs from PFFs-injected mice exhibited greater reduction in the amplitude towards the end of repetitive stimulation. n = 13-15 neurons/ 3 mice. **B1**) Representative cortico-BLA EPSCs traces from WT control and αSyn KO mice in response to repetitive stimulation (300 stimuli at 12.5 Hz). **B2**) Summarized graph showing the temporal profiles of cortico-EPSCs depression in slices from WT control and αSyn KO mice (n = 8-9 neurons/3 mice. *, $p < 0.05$, MWU followed by Bonferroni-Dunn correction for multiple comparisons).

Because both gain of toxic properties and loss of normal αSyn function were induced in the PFFs models, we employed the αSyn KO mice to further assess the impact of a loss of αSyn on the short-term synaptic plasticity of glutamatergic synapses. Consistently, the amplitude of cortico-BLA EPSCs from αSyn KO mice also exhibited greater depression in response to repetitive stimulation relative to littermate WT controls (Figure 4B1-B2), indicating an impaired mobilization of synaptic vesicle pools. It is worth noting that the earlier onset and greater magnitude of cortico-BLA EPSC depression in αSyn KO mice versus that in PFFs-injected mice (Figure 4A-B). Thus, it is plausible that the different temporary profiles of short-term synaptic dynamics are linked to difference in the amount of αSyn present at presynaptic terminals between the PFFs model and KO mice. Last, we did not detect difference in the temporal profiles of thalamo-BLA EPSCs in slices from αSyn KO mice and those from WT controls (Figure S1), which indicates a neglectable impact of αSyn depletion on synaptic vesicle dynamics and is consistent with the lack of αSyn presence at vGluT2^{+} axon terminals (Figure 1). Together, these results suggest that pathological aggregation decreases the levels of soluble αSyn at the axon terminals, leading to a greater synaptic vesicle depletion and impaired short-term plasticity.

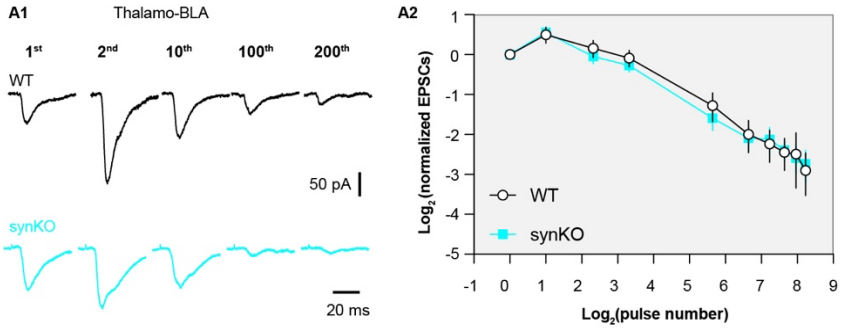

Figure S1. αSyn KO does not affect short term plasticity profiles of thalamo-BLA inputs. A1) Representative thalamo-BLA EPSCs traces from WT control and αSyn KO mice in response to repetitive stimulation (300 stimuli at 12.5 Hz). **A2**) Summarized graph showing the temporal profiles of thalamo-BLA EPSCs depression in slices from WT control and αSyn KO mice (n = 9 neurons/3 mice. No statistical significance was detected between groups, MWU followed by Bonferroni-Dunn correction for multiple comparisons).

Short-term synaptic plasticity is an important "gain control" mechanism for neurons to properly balance their responsiveness to distinct afferents in an input-specific manner (Abbott et al., 1997). Cortical and thalamic afferents of the BLA exhibit different short-term synaptic plasticity profiles *in vivo*, which could reflect their different contributions to the formation of emotion related memory and behavior (Siguròsson et al., 2010). Physiologically, synapse-specific presence of αSyn could underlie such difference in the short-term plasticity profiles of the two inputs. One can postulate that once aggregates form, a decreased synaptic strength associated with αSyn toxicity (Figure 2) and an enhanced synaptic depression due to the loss of αSyn normal function at presynaptic buttons (Figure 4) make the BLA neurons less likely to respond to sustained and repetitive sensory inputs from cortical regions. These circuit changes might explain studies showing a decreased functional connectivity of cortico-amygdala, but not the thalamo-amygdala network in PD patients, which further leads to a failed

amygdala responsiveness to the aversive sensory inputs (Hu et al., 2015; Yoshimura et al., 2005).

Materials and Methods

Animals

Wild type (WT) C57Bl/6 mice of both sexes (3 – 4 month-old) were obtained from the Van Andel Institute vivarium internal colony and used in the study. αSyn knockout (*Snca*$^{-/-}$) mice were originally purchased from Jackson laboratories (Bar Harbor, ME) and maintained in C57Bl/6 background. Experimental *Snca*$^{-/-}$ mice and littermate WT controls were generated from heterozygous *Snca*$^{+/-}$ breeder pairs and were genotyped by Transnetyx (Cordova, TN, USA). Mice were housed up to four animals per cage under a 12/12 h light/dark cycle with access to food and water *ad libitum* in accordance with NIH guidelines for care and use of animals. All animal studies were reviewed and approved by the Institutional Animal Care and Use Committee at Van Andel Institute.

Preparation and validation of αSyn preformed fibrils

Purification of recombinant mouse αSyn and generation of αSyn preformed fibrils (PFFs) was conducted as described elsewhere (Luk et al., 2009; Volpicelli-Daley et al., 2014). The pRK172 plasmid containing the gene of interest was transformed into BL21 (DE3) RIL-competent *E. coli* (230245, Agilent Technologies). A single colony from this transformation was expanded in Terrific Broth (12 g/L of Bacto-tryptone, 24 g/L of yeast extract 4% (v/v) glycerol, 17 mM KH_2PO_4 and 72 mM K_2HPO_4) with ampicillin. Bacterial pellets from the growth were sonicated and the sample was boiled to precipitate undesired proteins. The supernatant was dialyzed with 10 mM Tris, pH 7.6, 50 mM NaCl, 1 mM EDTA, 1 mM phenylmethylsulfonyl fluoride (PMSF) overnight. Protein was filtered with a 0.22 μm filter and concentrated using Vivaspin 15R 10K centrifugal filters

(VS15RH01, Sartorius). Protein was then loaded onto a Superdex 200 column and 2 mL fractions were collected. Fractions were run on SDS-PAGE and stained with InstaBlue protein stain (50-190-5499, Fisher Scientific) to select fractions that were highly enriched in αSyn. These fractions were combined and dialyzed in 10 mM Tris, pH 7.6, 50 mM NaCl, 1 mM EDTA, 1 mM PMSF overnight. Dialyzed fractions were applied to a MonoQ column (HiTrap Q HP 17115401, Cytiva) and run using a NaCl linear gradient (0.025-1 M). Collected fractions were run on SDS-PAGE and stained with InstaBlue protein stain. Fractions that were highly enriched in αSyn were collected and dialyzed into DPBS (Gibco). Protein was filtered through a 0.22 μm filter and concentrated to 7 mg/mL (αSyn) with Vivaspin 15R 10K centrifugal filters. Monomer was aliquoted and frozen at -80°C. For preparation of αSyn PFFs, αSyn monomer was shaken at 1,000 rpm for 7 days. Conversion to PFFs was validated by sedimentation at 100,000 *x g* for 60 minutes and by thioflavin S staining.

Stereotaxic surgery

Mice were placed in a stereotaxic frame (Kopf) under 2% isoflurane anesthesia and were supported by a thermostatic heating pad. Recombinant αSyn fibrils were diluted in phosphate-buffered saline (PBS) to a concentration of 5 mg/ml. Prior to stereotaxic injection, PFFs were pulse sonicated at medium intensity with 30 seconds on and 30 seconds off for 10 minutes using a sonicator (Biorupter Pico). To induce the formation of αSyn aggregation in mouse brain (Luk et al., 2012), sonicated PFFs (2.0 μl) were injected bilaterally into the dorsal striatum (anteroposterior, +0.2 mm from bregma; mediolateral, ±2.0 mm from the midline; dorsoventral, -2.6 mm from the brain surface)

using a 10-µl syringe (Hamilton) driven by a motorized microinjector (Stoelting) at a rate of 0.2 µl/min. Given the neuronal heterogeneity of the BLA, retrobeads (Lumafluor Inc) were diluted 10x into αSyn fibrils or PBS to label the projection neurons in the BLA for physiological studies. The final injection volume of PFFs with beads mixture was adjusted to keep a constant amount of αSyn injected across animals. Control mice received 2.0 µl PBS or PBS with retrobeads injections in the same location. For optogenetics studies, AAV vectors encoding ChR2(H134R)-eYFP (titer = 1 x 10^{12} vg/ml, Addgene 26973) were stereotaxically injected into and centered at the temporal association cortex (TeA) (anterioposterior -3.3 mm from the bregma, mediodorsal ±4.1 mm, dorsoventral -1.5 mm from the brain surface) and the midline thalamus (anterioposterior -1.5 mm from the bregma, mediodorsal 0 mm, dorsoventral -3.3 mm from the brain surface) (Ahmed et al., 2021; Amir et al., 2019). Animals were housed in their home cages before being euthanized for immunohistochemical or physiological studies at one-month post-injection.

Immunohistochemistry. Animals received overdosage of avertin intraperitoneally (i.p.) and were subsequently subjected to transcardial perfusion with PBS and 4% paraformaldehyde (PFA, pH 7.4). Brains were removed and post-fixed in 4% PFA overnight, before being re-sectioned at 70 µm using a vibratome (VT1000s, Leica Biosystems, Buffalo Grove, IL). Brain sections were then rinsed using PBS and treated with 0.5% Triton X-100 and 2% normal donkey serum (MilliporeSigma) in PBS for 60 min at room temperature, followed by incubation with primary antibodies overnight at room temperature or for 48 hours at 4 °C. The concentrations of primary antibodies

were rabbit anti-pS129 αSyn (1:10,000, cat#: EP1536Y, Abcam), mouse anti-αSyn (1:1,000, cat#: 610787, BDbiosciences), mouse anti-NeuN (1:2000, cat#: MAB377, MilliporeSigma), rabbit anti-vGlut1(1:1,000, cat#: ABN1647, MilliporeSigma) and guinea pig anti-vGluT2 (1:1000, cat#: 135404, SynapticSystems). After being thoroughly rinsed with PBS for 3 times, the sections were incubated with the secondary antibodies (1:500, AlexaFluor 594 or 647 donkey anti-mouse IgG, AlexaFluor 488 or 594 donkey anti-rabbit IgG, or AlexaFluor 488 donkey anti-guinea pig IgG, Jackson ImmunoResearch) for 90 min at room temperature. Brain sections were rinsed 3 times with PBS and mounted on glass slides using Vectorshield antifade mounting medium (H-1000, Vector Laboratories) and cover slipped.

Confocal imaging and analysis

Confocal images were acquired using a Nikon A1R confocal microscopy. pS129 αSyn aggregates in different brain regions were imaged under a 40x objective lens. For αSyn and vGluT1/vGluT2 colocalization analysis, three synaptic markers were immunostained simultaneously and z-stack images were acquired using an oil immersion 100x objective (NA = 1.45; x/y, 1024 X 1024 pixels; z step = 150 nm). Images were acquired using identical settings between treatment groups, including laser power, pinhole size, gain, and pixel size. Intensity-based colocalization analysis was performed using Imaris software (version 9.3, Oxford, UK). Background subtraction on z-stack images was conducted using ImageJ (NIH) prior to importing files into Imaris. Once imported, two arbitrary regions of interest were created using the surface function (drawing mode: circle; radius = 15 μm; number of vertices = 30) and the three channels

(vGluT2, vGluT1, αSyn) were masked based on the surface reconstruction to isolate fluorescence within the ROIs. The Imaris “Coloc” function was used to measure the colocalization between vGluT2/αSyn and vGluT1/αSyn for each ROI. Briefly, either vGluT1 or vGluT2 was selected as channel A and αSyn was selected as channel B. The automatic threshold feature within “Coloc” was used to calculate the threshold values for each channel. Colocalization channels for vGluT1/ αSyn and vGluT2/αSyn for each ROI were created by using the "Build Coloc Channel" function. Colocalization parameters were obtained for quantification from the colocalization channels. For quantification of the αSyn intensity within vGluT1$^+$ axon terminals, background subtraction on z-stack images was conducted using ImageJ (NIH). After background subtraction, vGluT1 immunoreactive puncta were manually identified as a set of regions of interest (ROI, n = 20 puncta per image) from each BLA section and the mean gray values of αSyn immunoreactivity within the same ROI were then measured using ImageJ (NIH).

Slice preparation for physiology. For physiological studies, mice were deeply anesthetized with avertin (300 mg/kg, i.p.) and then were perfused transcardially with ice-cold, sucrose-based artificial cerebrospinal fluid (aCSF) containing (in mM) 230 sucrose, 26 $NaHCO_3$, 10 glucose, 10 $MgSO_4$, 2.5 KCl, 1.25 NaH_2PO_4, and 0.5 $CaCl_2$, 1 sodium pyruvate, and 0.005 L-glutathione. Next, coronal brain slices (300 μm) containing BLA were prepared in the same sucrose-based aCSF solution using a vibratome (VT1200S; Leica Microsystems, Buffalo Grove, IL). Brain slices were kept in normal aCSF (in mM, 126 NaCl, 26 $NaHCO_3$, 10 glucose, 2.5 KCl, 2 $CaCl_2$, 2 $MgSO_4$,

1.25 NaH_2PO_4, 1 sodium pyruvate, and 0.005 L-glutathione) equilibrated with 95% O_2 and 5% CO_2 for 30 min at 35°C and then held at room temperature until use.

Ex vivo electrophysiology recording and optogenetics. Brain slices were transferred into a recording chamber perfused at a rate of 3 – 4 ml/min with synthetic interstitial fluid (in mM, 126 NaCl, 26 $NaHCO_3$,10 glucose, 3 KCl, 1.6 $CaCl_2$,1.5 $MgSO_4$, and1.25 NaH_2PO_4) equilibrated with 95% O_2 and 5% CO_2 at 33–34°C via a feedback-controlled in-line heater (TC-324C, Warner Instruments) (Chen et al., 2021). SR-95531 (GABAzine, 10 μM) was routinely added extracellularly to block $GABA_A$ receptor-mediated inhibitory synaptic transmission. Neurons were visualized and recorded under gradient contrast SliceScope 1000 (Scientifica, Uckfield, UK) with infrared illumination using an IR-2000 CCD camera (DAGE-MTI, USA) and motorized micromanipulators (Scientifica, Uckfield, UK). Individual BLA projection neurons labeled with retrobeads were identified using a 60x water immersion objective lens (Olympus, Japan) and targeted for whole-cell patch-clamp recording. Data were collected using a MultiClamp 700B amplifier and a Digidata 1550B digitizer at a sampling rate of 50 kHz under the control of pClamp11 (Molecular Devices, San Jose, USA). Borosilicate glass pipettes (O.D. = 1.5 mm, I.D. = 0.86 mm, item #BF150-86-10, Sutter Instruments) for patch clamp recordings (4 – 6 MΩ) were pulled using a micropipette puller (P1000, Sutter Instruments, Novato, CA).

To assess glutamatergic transmission in the BLA, glass pipettes were filled with a cesium methanesulfonate based internal solution of (in mM): 120 CH_3O_3SCs, 2.8 NaCl, 10 HEPES, 0.4 Na_4-EGTA, 5 QX314-HBr, 5 phosphocreatine, 0.1 spermine, 4 ATP-Mg,

and 0.4 GTP-Na (pH 7.3, 290 mOsm). BLA neurons were voltage clamped at -70 mV to assess the excitatory postsynaptic currents (EPSCs) in response to presynaptic electrical or optogenetic stimulations. Concentric bipolar electrodes (FHC, Bowdoin, ME) or glass pipettes (~ 2 MΩ) filled with the extracellular solution were used as stimulating electrodes and placed on the external and internal capsules to evoke glutamate release in the BLA from cortical and thalamic axon terminals, respectively (Shin et al., 2010). A range of electrical pulses (intensities = 30 – 120 μA, duration = 100 μs) were delivered through a stimulator (Digitimer, UK) to evoke glutamate release at either cortical or thalamic inputs. To study the process of synaptic vesicle pool mobilization during repetitive glutamatergic transmission, we delivered 300 electrical pulses (duration = 100 μs) at 12.5 Hz and measured the amplitudes of EPSCs to quantify changes in the presynaptic glutamate release (Cabin et al., 2002). Only one neuron was recorded from each slice in the prolonged repetitive stimulation studies.

Optogenetic stimulation pulses (1 ms duration) were delivered through a 60x objective lens (Olympus, Japan) using a 470 nm LED light source (CoolLED, UK). To isolate monosynaptic cortico-BLA and thalamo-BLA EPSCs, optogenetically evoked EPSCs were recorded in the presence of TTX (1 μM) and 4-AP (100 μM). Series resistance (Rs, < 20 MΩ) was regularly monitored throughout the recording to ensure Rs changes were less than 15%. Liquid junction potential (~ 9 mV) was not corrected.

Data analysis and statistics.

Electrophysiology data were analyzed offline in Clampfit 11.1 (Molecular Devices). The peak amplitude of monosynaptic EPSCs in response to electric stimulation was

quantified from an average of three to five sweeps. Digital confocal images were analyzed using ImageJ (NIH) or Imaris (Oxford,UK). Statistics were perform using Prism9 (GraphPad Software). To minimize the assumption of the data normality, non-parametric, distribution-independent Mann–Whiney U (MWU) test was used for non-paired data comparisons between groups, followed by Bonferroni-Dunn correction for multiple comparisons. All tests were two-tailed, and p value < 0.05 was considered statistically significant. Summary results are reported as mean plus standard error of mean.

References

Abbott, L.F., and Regehr, W.G. (2004). Synaptic computation. Nature *431*, 796–803.

Abbott, L.F., Varela, J.A., Sen, K., and Nelson, S.B. (1997). Synaptic Depression and Cortical Gain Control. Science *275*, 221–224.

Abeliovich, A., Schmitz, Y., Fariñas, I., Choi-Lundberg, D., Ho, W.-H., Castillo, P.E., Shinsky, N., Verdugo, J.M.G., Armanini, M., Ryan, A., et al. (2000). Mice Lacking α-Synuclein Display Functional Deficits in the Nigrostriatal Dopamine System. Neuron *25*, 239–252.

Ahmed, N., Headley, D.B., and Paré, D. (2021). Optogenetic study of central medial and paraventricular thalamic projections to the basolateral amygdala. J Neurophysiol *126*, 1234–1247.

Alabi, A.A., and Tsien, R.W. (2012). Synaptic Vesicle Pools and Dynamics. Csh Perspect Biol *4*, a013680.

Amir, A., Paré, J., Smith, Y., and Paré, D. (2019). Midline thalamic inputs to the amygdala: Ultrastructure and synaptic targets. J Comp Neurol *527*, 942–956.

Angot, E., Steiner, J.A., Hansen, C., Li, J.-Y., and Brundin, P. (2010). Are synucleinopathies prion-like disorders? Lancet Neurology *9*, 1128–1138.

Benskey, M.J., Perez, R.G., and Manfredsson, F.P. (2016). The contribution of alpha synuclein to neuronal survival and function – Implications for Parkinson's disease. J Neurochem *137*, 331–359.

Bowers, D., Miller, K., Mikos, A., Kirsch-Darrow, L., Springer, U., Fernandez, H., Foote, K., and Okun, M. (2006). Startling facts about emotion in Parkinson's disease: blunted reactivity to aversive stimuli. Brain *129*, 3356–3365.

Buck, S.A., Miranda, B.R.D., Logan, R.W., Fish, K.N., Greenamyre, J.T., and Freyberg, Z. (2021). VGLUT2 Is a Determinant of Dopamine Neuron Resilience in a Rotenone Model of Dopamine Neurodegeneration. J Neurosci *41*, 4937–4947.

Burré, J., Sharma, M., Tsetsenis, T., Buchman, V., Etherton, M.R., and Südhof, T.C. (2010). α-Synuclein Promotes SNARE-Complex Assembly in Vivo and in Vitro. Science *329*, 1663–1667.

Burtscher, J., Copin, J.-C., Rodrigues, J., Kumar, S.T., Chiki, A., Suduiraut, M.-I.G. de, Sandi, C., and Lashuel, H.A. (2019). Chronic corticosterone aggravates behavioural and neuronal symptomatology in a mouse model of alpha-synuclein pathology. Neurobiol Aging *83*, 11–20.

Cabin, D.E., Shimazu, K., Murphy, D., Cole, N.B., Gottschalk, W., McIlwain, K.L., Orrison, B., Chen, A., Ellis, C.E., Paylor, R., et al. (2002). Synaptic Vesicle Depletion Correlates with Attenuated Synaptic Responses to Prolonged Repetitive Stimulation in Mice Lacking α-Synuclein. J Neurosci *22*, 8797–8807.

Cookson, M.R., and Brug, M. van der (2008). Cell systems and the toxic mechanism(s) of α-synuclein. Exp Neurol *209*, 5–11.

Erskine, D., Patterson, L., Alexandris, A., Hanson, P.S., McKeith, I.G., Attems, J., and Morris, C.M. (2018). Regional levels of physiological α-synuclein are directly associated with Lewy body pathology. Acta Neuropathol *135*, 153–154.

Fremeau, R.T., Troyer, M.D., Pahner, I., Nygaard, G.O., Tran, C.H., Reimer, R.J., Bellocchio, E.E., Fortin, D., Storm-Mathisen, J., and Edwards, R.H. (2001). The Expression of Vesicular Glutamate Transporters Defines Two Classes of Excitatory Synapse. Neuron *31*, 247–260.

Harding, A.J., Stimson, E., Henderson, J.M., and Halliday, G.M. (2002). Clinical correlates of selective pathology in the amygdala of patients with Parkinson's disease. Brain J Neurology *125*, 2431–2445.

Henderson, M.X., Cornblath, E.J., Darwich, A., Zhang, B., Brown, H., Gathagan, R.J., Sandler, R.M., Bassett, D.S., Trojanowski, J.Q., and Lee, V.M.Y. (2019). Spread of α-synuclein pathology through the brain connectome is modulated by selective vulnerability and predicted by network analysis. Nat Neurosci *22*, 1248–1257.

Hu, X., Song, X., Yuan, Y., Li, E., Liu, J., Liu, W., and Liu, Y. (2015). Abnormal functional connectivity of the amygdala is associated with depression in Parkinson's disease. Movement Disord *30*, 238–244.

Janak, P.H., and Tye, K.M. (2015). From circuits to behaviour in the amygdala. Nature *517*, 284–292.

Kaneko, T., and Fujiyama, F. (2002). Complementary distribution of vesicular glutamate transporters in the central nervous system. Neurosci Res *42*, 243–250.

Luk, K.C., Song, C., O'Brien, P., Stieber, A., Branch, J.R., Brunden, K.R., Trojanowski, J.Q., and Lee, V.M.-Y. (2009). Exogenous α-synuclein fibrils seed the formation of Lewy body-like intracellular inclusions in cultured cells. Proc National Acad Sci USA *106*, 20051–20056.

Luk, K.C., Kehm, V., Carroll, J., Zhang, B., O'Brien, P., Trojanowski, J.Q., and Lee, V.M.-Y. (2012). Pathological α-Synuclein Transmission Initiates Parkinson-like Neurodegeneration in Nontransgenic Mice. Science *338*, 949–953.

Mezey, E., Dehejia, A.M., Harta, G., Suchy, S.F., Nussbaum, R.L., Brownstein, M.J., and Polymeropoulos, M.H. (1998). Alpha synuclein is present in Lewy bodies in sporadic Parkinson's disease. Mol Psychiatr *3*, 493–499.

Nelson, P.T., Abner, E.L., Patel, E., Anderson, S., Wilcock, D.M., Kryscio, R.J., Eldik, L.J.V., Jicha, G.A., Gal, Z., Nelson, R.S., et al. (2017). The Amygdala as a Locus of Pathologic Misfolding in Neurodegenerative Diseases. J Neuropathology Exp Neurology *77*, 2–20.

Runwal, G., and Edwards, R.H. (2021). The Membrane Interactions of Synuclein: Physiology and Pathology. Annu Rev Pathology Mech Dis *16*, 465–485.

Shin, R.-M., Tully, K., Li, Y., Cho, J.-H., Higuchi, M., Suhara, T., and Bolshakov, V.Y. (2010). Hierarchical order of coexisting pre- and postsynaptic forms of long-term potentiation at synapses in amygdala. Proc National Acad Sci *107*, 19073–19078.

Siguròsson, T., Sigurdsson, T., Cain, C.K., Doyère, V., and LeDoux, J.E. (2010). Asymmetries in long-term and short-term plasticity at thalamic and cortical inputs to the amygdala in vivo. Eur J Neurosci *31*, 250–262.

Sorrentino, Z.A., Goodwin, M.S., Riffe, C.J., Dhillon, J.-K.S., Xia, Y., Gorion, K.-M., Vijayaraghavan, N., McFarland, K.N., Golbe, L.I., Yachnis, A.T., et al. (2019). Unique α-synuclein pathology within the amygdala in Lewy body dementia: implications for disease initiation and progression. Acta Neuropathologica Commun *7*, 142.

Spillantini, M.G., Schmidt, M.L., Lee, V.M.-Y., Trojanowski, J.Q., Jakes, R., and Goedert, M. (1997). α-Synuclein in Lewy bodies. Nature *388*, 839–840.

Stoyka, L.E., Arrant, A.E., Thrasher, D.R., Russell, D.L., Freire, J., Mahoney, C.L., Narayanan, A., Dib, A.G., Standaert, D.G., and Volpicelli-Daley, L.A. (2019). Behavioral defects associated with amygdala and cortical dysfunction in mice with seeded α-synuclein inclusions. Neurobiol Dis 104708.

Sulzer, D., and Edwards, R.H. (2019). The physiological role of α-synuclein and its relationship to Parkinson's Disease. J Neurochem *150*, 475–486.

Surmeier, D.J., Obeso, J.A., and Halliday, G.M. (2017). Selective neuronal vulnerability in Parkinson disease. Nat Rev Neurosci *18*, 101–113.

Thakur, P., Chiu, W.H., Roeper, J., and Goldberg, J.A. (2019). α-SYNUCLEIN 2.0 – Moving towards Cell-Type Specific Pathophysiology. Neuroscience *412*, 248–256.

Thomas, S., S, C., William, Imre, K., A, R., Robert, B, L., Edward, Q, T., John, Zachary, F., Subhojit, R., C, L., Kelvin, M, L., Virginia, et al. (2021). Dopamine neurons exhibit emergent glutamatergic identity in Parkinson's disease. Brain awab373.

Uemura, N., Uemura, M.T., Luk, K.C., Lee, V.M.-Y., and Trojanowski, J.Q. (2020). Cell-to-Cell Transmission of Tau and α-Synuclein. Trends Mol Med *26*, 936–952.

Vargas, K.J., Schrod, N., Davis, T., Fernandez-Busnadiego, R., Taguchi, Y.V., Laugks, U., Lucic, V., and Chandra, S.S. (2017). Synucleins Have Multiple Effects on Presynaptic Architecture. Cell Reports *18*, 161–173.

Vasili, E., Dominguez-Meijide, A., Flores-León, M., Al-Azzani, M., Kanellidi, A., Melki, R., Stefanis, L., and Outeiro, T.F. (2022). Endogenous Levels of Alpha-Synuclein Modulate Seeding and Aggregation in Cultured Cells. Mol Neurobiol 1–12.

Vigneault, É., Poirel, O., Riad, M., Prud'homme, J., Dumas, S., Turecki, G., Fasano, C., Mechawar, N., and Mestikawy, S.E. (2015). Distribution of vesicular glutamate transporters in the human brain. Front Neuroanat *9*, 23.

Volpicelli-Daley, L.A., Luk, K.C., Patel, T.P., Tanik, S.A., Riddle, D.M., Stieber, A., Meaney, D.F., Trojanowski, J.Q., and Lee, V.M.-Y. (2011). Exogenous α-Synuclein Fibrils Induce Lewy Body Pathology Leading to Synaptic Dysfunction and Neuron Death. Neuron *72*, 57–71.

Volpicelli-Daley, L.A., Luk, K.C., and Lee, V.M.-Y. (2014). Addition of exogenous α-synuclein preformed fibrils to primary neuronal cultures to seed recruitment of endogenous α-synuclein to Lewy body and Lewy neurite–like aggregates. Nat Protoc *9*, 2135–2146.

Yoshimura, N., Kawamura, M., Masaoka, Y., and Homma, I. (2005). The amygdala of patients with Parkinson's disease is silent in response to fearful facial expressions. Neuroscience *131*, 523–534.

Ziolkowska, B., Gieryk, A., Bilecki, W., Wawrzczak-Bargiela, A., Wedzony, K., Chocyk, A., Danielson, P.E., Thomas, E.A., Hilbush, B.S., Sutcliffe, J.G., et al. (2005). Regulation of α-Synuclein Expression in Limbic and Motor Brain Regions of Morphine-Treated Mice. J Neurosci *25*, 4996–5003.